AIAA JOURNAL
Vol. 38, No. 5, May 2000

Flange Delamination Prediction in Composite Structures with Ply Waviness

Jian Li*
The Boeing Company, Mesa, Arizona 85215-9797

A fracture-mechanics-based delamination prediction strategy for load-carrying composite structures is proposed. This strategy relies on the knowledge of failure modes and local structural details to predict failure based on coupon-level test data. The methodology presented effectively predicted delamination initiation of a composite hat stringer based on fracture toughness test data. In addition, ply waviness was identified as a critical factor influencing the delamination failure load. The finite element modeling technique was used to model the skin-flange region, which included the ply waviness effect. The finite element analysis results were used to calculate the total strain energy release rate and its mode I and II components. The finite element analysis predicted unstable delamination growth for positive waviness angles and stable delamination growth for negative waviness angles. The same trends for the relationship between ply waviness angle and the critical load for delamination initiation were observed in the pull-off specimens previously tested. The predictions captured the trend of the test results.

Introduction

ADVANCED composite structures are being developed as primary structures for next generation aircraft and rotorcraft for weight and cost savings and other gains related to the use of composites. However, the cost savings cannot be realized by directly adopting the building block approach for isotropic materials to composite structures because an enormous amount of testing is required to certify the composite structures. A change in ply orientations could render most of the test results useless. The versatility of composite materials also exhibits multiple failure modes unique to composite structures, such as delamination and matrix cracking. Any attempt to predict failure in composite structures without taking into account individual failure modes will not be able to go beyond curve fitting test data.

One of the failure modes observed in advanced composite structures is skin-stiffener debonding or delamination induced by skin buckling (Fig. 1). The flange delamination shown in Fig. 1 is one of many failure modes that the structural analyst must check. An example is the skin-flange debonding/delamination of a composite hat stringer developed for tiltrotor wing and fuselage applications.[1] Hat stringer pull-off tests were performed to simulate the delamination failure mechanism in the skin-flange region (Fig. 2).[2]

A fracture mechanics approach with a mixed mode delamination criterion accurately predicted pull-off loads.[2] The secret to this success is an analytical methodology that takes into account the as-manufactured local details of each individual specimen, such as ply termination, resin pockets, and ply waviness at the critical location. However, this level of detailed analysis may not be practical in the design process in industry. It is also not necessary once the dominant factor affecting failure initiation is identified. The waviness angle at the delamination initiation location was identified and analyzed using the mixed-mode split (MMS) local finite element model configuration.[3] The MMS configuration is similar to the well-known double cantilever beam (DCB) test, but with only one of the beams under loading (Fig. 3).

The local finite element model of the MMS configuration captured the ply waviness effects on the delamination initiation and associated critical load and illustrated that very small angles corresponding to a modest amount of ply waviness at the delamination front lead to significant changes in the delamination initiation loads. However, the ply waviness effect is much more pronounced on the delamination initiation load for the MMS than the pull-off load for the pull-off specimen. Hence, the MMS configuration could not be used to predict the skin-flange delamination directly.

In this paper, the skin-flange delamination initiation issue (due to pull-off loads) is further studied, and a prediction strategy is presented. The analytical predictions are developed based on an idealized model, but included the ply waviness effect.

Failure Prediction Methodology

The failure modes observed in the pull-off tests[2] were dominantly delamination between skin ply and flange ply starting from a resin crack for the cocured toughened epoxy composite skin stringer (Fig. 4). For cobonded skin stringers, both debonding at the bondline or delamination in the skin plies are possible failure modes (Fig. 5). The analysis is applied to the failure mode shown in Fig. 4, but it is also applicable to the failure modes shown in Fig. 5 with some modifications.

Fracture Mechanics Approach

The failure modes shown in Figs. 4 and 5 are best analyzed by a fracture mechanics approach. The failure mode shown in Fig. 4 indicates a resin crack is formed preceding the delamination initiation and growth that fails the pull-off specimen. Hence, it is assumed that a crack has formed in between the resin pocket and the ply termination before delamination initiation and growth. The failure prediction in this case is simplified to the prediction of delamination initiation and growth. The strain energy release rate is most often used to analyze composite delaminations. The strain energy release rate is the measure of the loss of strain energy as new delamination surface area is created. Delaminations are typically mixed-mode-fracture phenomena, consisting of a combination of an opening mode I, due to interlaminar tension, a sliding shear mode II, due to interlaminar shear, and a scissoring shear mode III, due to antiplane shear. The total strain energy release rate G_T consists of contributions due to opening mode fracture G_I, sliding shear fracture G_{II}, and scissoring shear fracture G_{III}. Hence, $G_T = G_I + G_{II} + G_{III}$. Test methods have been proposed in the past to characterize fracture toughness in each of the three delamination modes. A comparison of the delamination onset strain energy release rate or fracture toughness among the three delamination modes is given in Ref. 4. For the symmetric balanced layups considered here, the extension–twist and bending–twist couplings are negligible. Hence, under the plane loading state introduced here, $G_{III} = 0$, $G_T = G_I + G_{II}$, and the delamination initiation is governed by G_T and mixed-mode ratio (G_{II}/G_T). To implement the fracture mechanics analysis, a finite element model is required to calculate G_T and G_{II}/G_T. Delamination initiates when

Presented as Paper 98-5570 at the AIAA/SAE 1998 World Aviation Conference, Anaheim, CA, 28–30 September 1998; received 30 October 1998; revision received 3 October 1999; accepted for publication 8 October 1999.

*Structures Analyst, Structural Integrity Department.

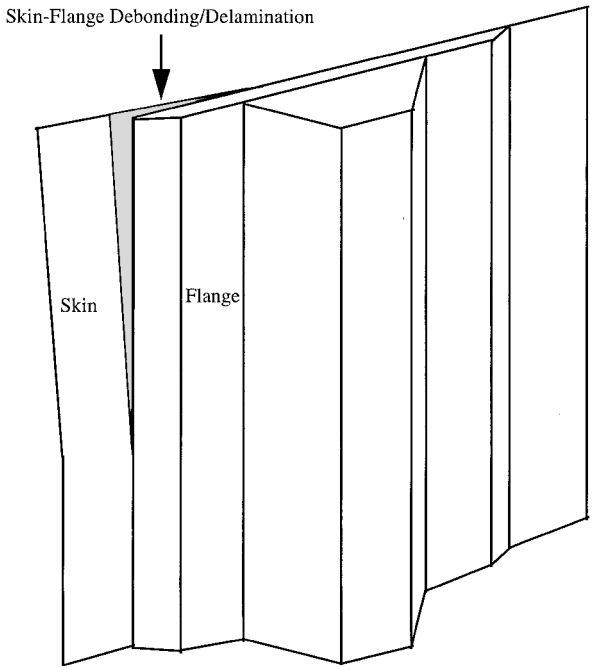

Fig. 1 Skin buckling-induced flange-skin debonding.

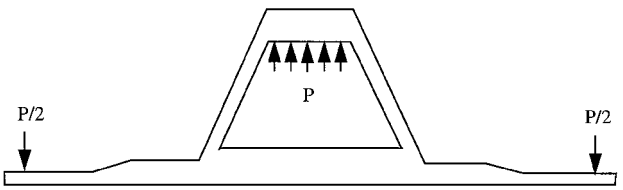

Fig. 2 Hat-stringer pull-off test.

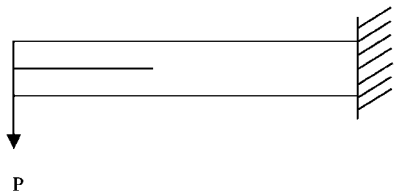

Fig. 3 MMS configuration.

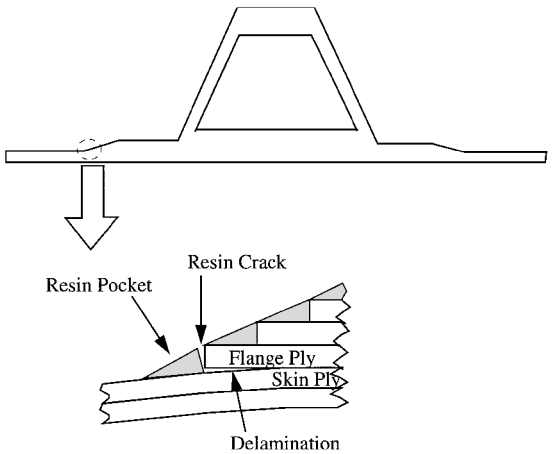

Fig. 4 Skin-flange delamination failure mode.

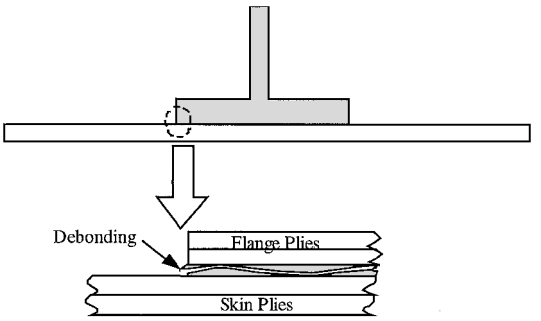

a) Debonding failure

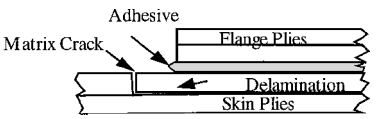

b) Matrix crack and delamination failure

Fig. 5 Other skin-flange debonding or delamination failure modes.

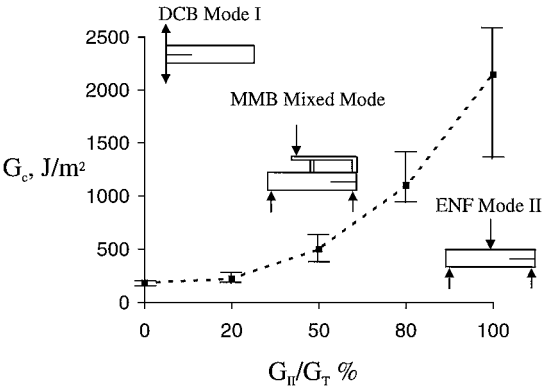

Fig. 6 Development of mixed-mode criterion.

the applied G_T reaches the material fracture toughness G_c at the applied mixed-mode ratio. To sum up into a mathematical expression,

$$G_T(G_{II}/G_T) = G_c(G_{II}/G_T) \quad (1)$$

For the pull-off tests, G_T is proportional to the square of the applied load P, that is,

$$G_T = \lambda P^2 \quad (2)$$

where λ is the constant of proportionality determined from the finite element analysis. Hence, the critical load P_c at delamination initiation is calculated as

$$P_c = \sqrt{G_c/\lambda} \quad (3)$$

Mixed-Mode Fracture Toughness

Figure 6 demonstrates the development of the mixed-mode fracture toughness data. The data for IM7/E7T1-2 graphite/epoxy unidirectional composites shown in Fig. 6 were generated from a round robin series of interlaboratory tests conducted within the American Society for Testing and Materials Committee D-30 on composites. The average mixed-mode fracture toughness along with the scatter ranges is plotted against the mixed mode ratio G_{II}/G_T. When the mixed-mode ratio is zero, the toughness value is the mode I fracture toughness G_{Ic} obtained from the DCB test. Pure mode II corresponds to the mode II fracture toughness G_{IIc} obtained from the end notch flexure (ENF) test. In between these extremes, the mixed mode bending (MMB) test[5] was used to generate the mixed-mode toughness values. An equation resulting from a regression cubic curve fit to these test data defines the mixed-mode delamination fracture toughness for each mixed-mode ratio. The cubic fit to the data shown in Fig. 6 is given by

$$G_c = M_0 + M_1(G_{II}/G_T) + M_2(G_{II}/G_T)^2 + M_3(G_{II}/G_T)^3 \quad (4)$$

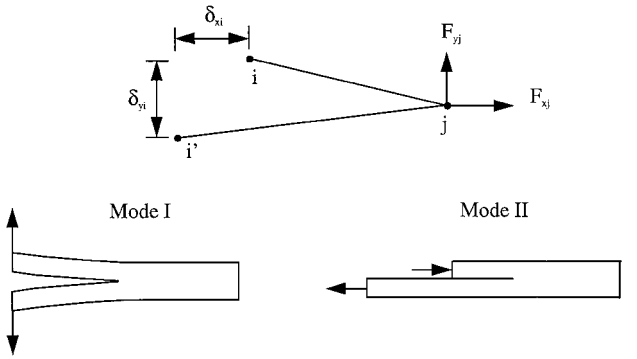

Fig. 7 Mode I and II strain energy release rates.

where the fitting parameters are $M_0 = 167.49$ Jm^{-2}, $M_1 = 439.65$ Jm^{-2}, $M_2 = -688.98$ Jm^{-2}, and $M_3 = 2207.5$ Jm^{-2}, respectively. The discrepancies in M_1–M_3 between here and Ref. 3 are in the location of the decimal point only, which is the result of the differences in unit definition for (G_{II}/G_T). The unit of (G_{II}/G_T) in Eq. (1) of Ref. 3 is in percentage (% or $G_{II}/G_T \times 100$) instead of (G_{II}/G_T).

Strain Energy Release Rate Components

As the preceding sections demonstrated, two of the three quantities, G_T, G_I, and G_{II}, need to be determined from finite element analysis. The virtual crack closure technique (VCCT)[6] is often used in numerical methods to calculate the strain energy release rate components. The VCCT uses the nodal forces ahead of the delamination front and the displacements behind the front to determine the strain energy release rate components. A simple formula for calculating the strain energy release rate components for a two-dimensional four-node element was given by Rybicki and Kanninen[7] and is briefly described here for completeness. This formula uses the forces at the crack tip and the relative displacements of the crack faces behind the crack tip to calculate the mode I and II components. The strain energy release rate components can be calculated from the work required to close the delamination by one element length $\triangle a$ (Fig. 7) as

$$G_I = \frac{F_{yj}\delta_{yi}}{2\triangle a} \tag{5}$$

$$G_{II} = \frac{F_{xj}\delta_{xi}}{2\triangle a} \tag{6}$$

where F_{xj} and F_{yj} are the forces in the x direction and y direction at node j and δ_{xi} and δ_{yi} are the relative crack face displacements between nodes i and i', located at a distance $\triangle a$ behind the crack tip in the x direction and y direction, respectively.

Finite Element Analysis

The skin and flange are assumed to consist of 10 ± 45-deg plies each of IM7/E7T1-2 graphite/epoxy tape. The material properties for unidirectional IM7/E7T1-2 lamina and E7T1-2 neat resin are given in Table 1. The transverse shear modulus G_{23} is assumed to be $G_{23} = V_f \times G_{12} = 0.6 \times 5.52 = 3.31$ GPa, and Poisson's ratio ν_{23} is calculated from $\nu_{23} = (E_{22}/2G_{23} - 1) = 0.46$, where V_f is the fiber volume fraction. In the following cross section modeling, the three-dimensional lamina properties are converted to two-dimensional cross section properties using the classical lamination theory. For simplicity, the ±45 layups are converted into two-dimensional orthotropic cross section properties given in Table 2, where subscript x denotes the in-plane coordinate axis and y denotes the through-thickness local coordinate axis.

Finite Element Models

A typical finite element model of the skin-flange region on one side of the hat stringer is shown in Fig. 8. The critical region where the delamination initiates is at the skin-flange built-up area on either side of the stiffener. Hence, only a section of the skin and flange on one side of the hat stringer is modeled. A statically equivalent clamped boundary condition is placed at the cutoff location. As shown in Fig. 8, the lengths of the skin region, the tapered region, and the flange region are denoted as L_1, L_2, and L_3, respectively. In this study these length dimensions are assumed to be $L_1 = 25.4$ mm, $L_2 = 12.7$ mm, and $L_3 = 12.7$ mm. Figure 9 shows the materials property sets at the critical location, where the shaded triangles represent resin pockets and the darkest inclined rectangle region represents ply waviness. A closeup look of the deformed shape at the critical location illustrates the resin crack and delamination as shown in Fig. 10. The finite element mesh consists mostly of four-noded quadrilateral shell elements (CQUAD4). The point circles in Fig. 10 denote double nodes with fixed multipoint constraints. The multipoint constraints were released systematically to calculate the strain energy release rate components as a function of delamination length a. Convergence was evaluated by refining the elements around the delamination tip region. There were no significant changes in the calculated mode I and II strain energy release rate components from an initial element length of one-half of a ply thickness down to a quarter of a ply thickness. Subsequently, a half-ply thickness element length was used in the delamination tip region for all of the models.

Table 1 IM7/E7T1-2 lamina properties

Material	Property
IM7/E7T1-2	E_{11} = 163 GPa (23.6 msi) $E_{22} = E_{33}$ = 9.65 GPa (1.4 msi) $G_{12} = G_{13}$ = 5.52 GPa (0.8 msi) $\nu_{12} = \nu_{13}$ = 0.33
Ply thickness	h = 0.214 mm (0.00843 in.)
E7T1-2 resin	E = 3.45 GPa (0.5 msi) ν = 0.41

Table 2 IM7/E7T1-2 cross-section properties

Property	Value
E_{xx}	19.7 GPa (2.85 msi)
E_{yy}	11.7 GPa (1.7 msi)
G_{xy}	4.42 GPa (0.64 msi)
ν_{xy}	0.104

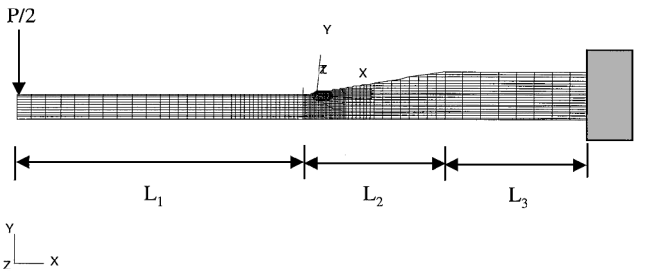

Fig. 8 Finite element model of the skin and flange.

The rectangular coordinate system at the corner of Figs. 8 or 9 is the global coordinate system, whereas the rotated rectangle coordinate system at the tip of the tapered region is the local coordinate system. The ply waviness angle is defined as the minimum angle rotated (counterclockwise positive) from the local x axis to the global x axis. The positive ply waviness angle is shown in Fig. 9. The modes I and II strain energy release rate components for the inclined delamination are calculated from

$$G_I = (1/2\triangle a)\left(F_{yj}\delta_{yi}\cos^2\alpha + F_{xj}\delta_{xi}\sin^2\alpha\right) + (1/2\triangle a)(F_{yj}\delta_{xi} + F_{xj}\delta_{yi})\sin\alpha\cos\alpha \tag{7}$$

$$G_{II} = (1/2\triangle a)\left(F_{yj}\delta_{yi}\sin^2\alpha + F_{xj}\delta_{xi}\cos^2\alpha\right) - (1/2\triangle a)(F_{yj}\delta_{xi} + F_{xj}\delta_{yi})\sin\alpha\cos\alpha \tag{8}$$

where α is the ply waviness. The forces and displacements in Eqs. (7) and (8) are in terms of global coordinates.

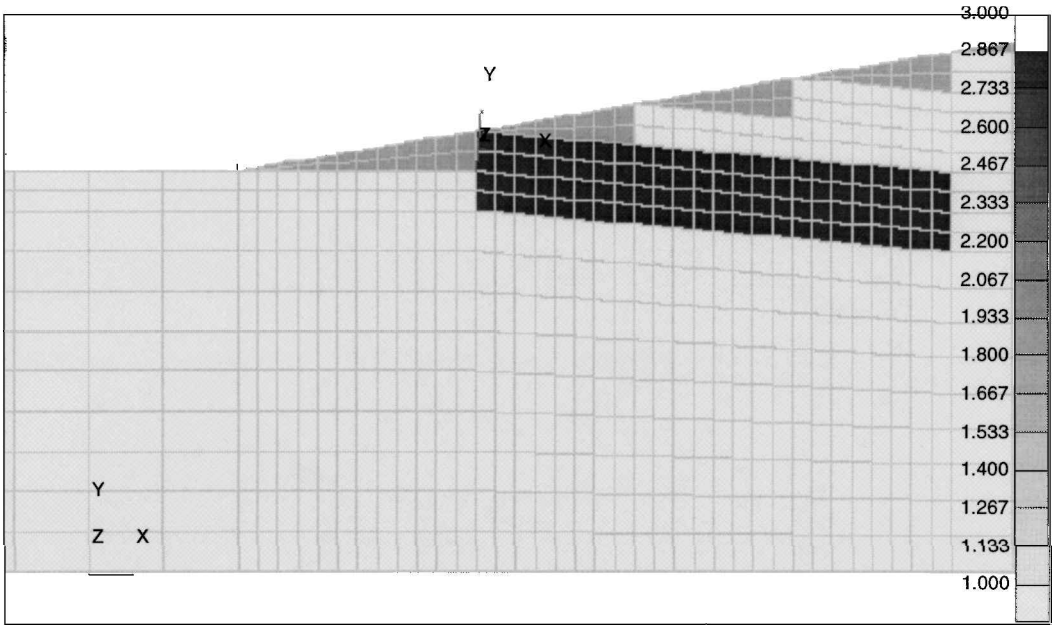

Fig. 9 Material property sets for the skin-flange region.

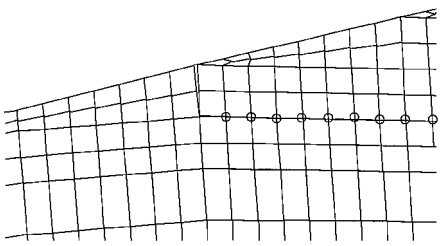

Fig. 10 Deformed shape of crack and delamination.

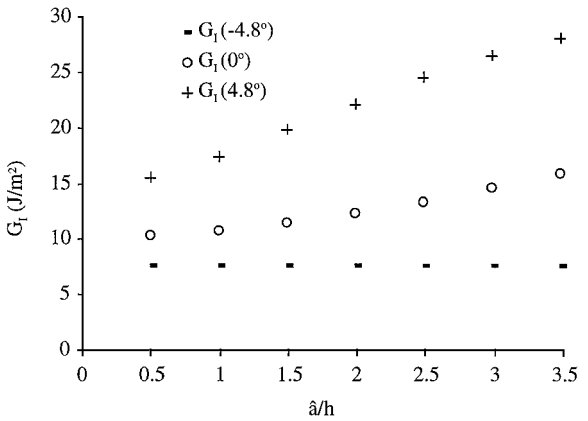

Fig. 11 Mode I strain energy release rate.

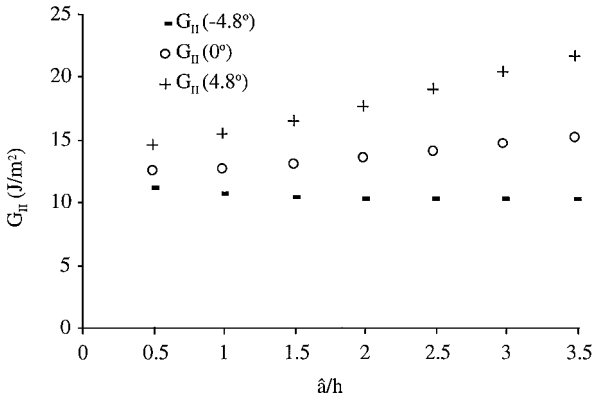

Fig. 12 Mode II strain energy release rate.

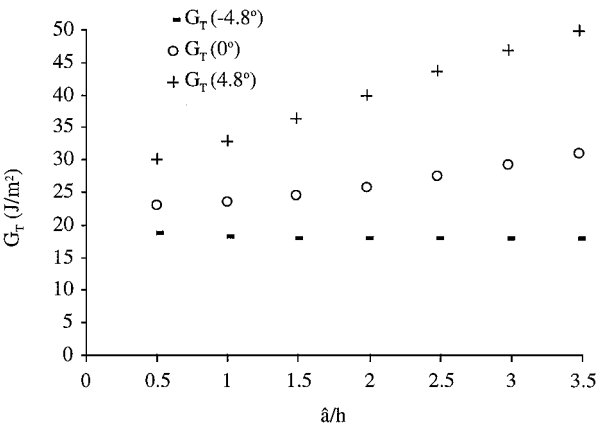

Fig. 13 Total strain energy release rate.

Strain Energy Release Rate

The total strain energy release rate and mode I and II components are calculated for three different ply waviness angles under an assumed load $P/2 = 1.75$ kN/m (10 lb/in.). These waviness angles are 4.8, 0, and −4.8 deg. The mode I and II components G_I and G_{II}, the total strain energy release rate G_T, and the mixed mode ratio G_{II}/G_T are plotted in Figs. 11–14, where $\hat{a}$ is the projection of delamination length a to the global x axis. As the ply waviness angle changes from negative (−4.8 deg) to positive (4.8 deg), Figs. 11–13 indicate increasing mode I, mode II, and total strain energy release rate, whereas Fig. 14 shows decreasing mixed-mode ratio G_{II}/G_T. Hence, as the ply waviness angle increases from −4.8 to 4.8 deg, the delamination initiation load decreases. As the delamination length increases, the mode I and II strain energy release rate components and the total strain energy release rate increase for 4.8- and 0-deg ply waviness angles, whereas they decease slightly for the −4.8-deg angle. This indicates unstable delamination growth for 4.8- and 0-deg ply waviness angles and stable delamination growth for −4.8 deg.

Delamination Prediction

After the determination of the mixed mode ratio G_{II}/G_T, the corresponding critical strain energy release rate can be determined

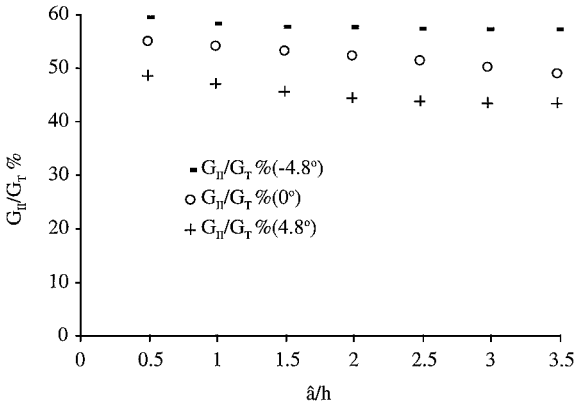

Fig. 14 Mode II to total strain energy release rate.

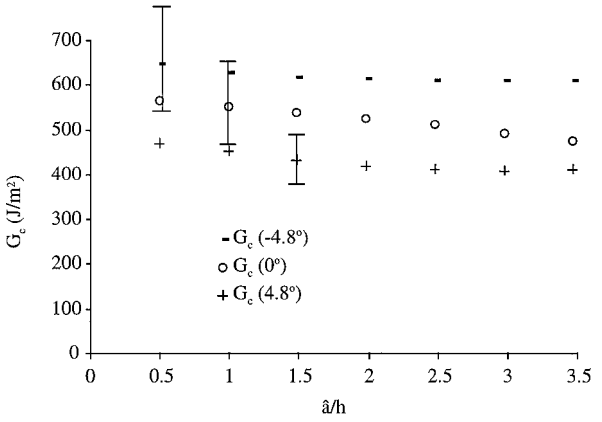

Fig. 15 Critical strain energy release rate.

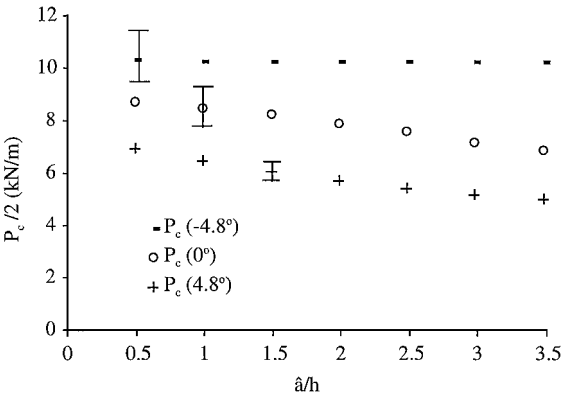

Fig. 16 Critical delamination initiation load.

from Eq. (4). Figure 15 shows the critical strain energy release rate as a function of delamination length for the G_{II}/G_T ratios shown in Fig. 14. This reflects that higher G_{II}/G_T has higher G_c. Three schematic scatter bars are shown in Fig. 15 to reflect the uncertainty due to the MMB data scatter, as shown in Fig. 6.

The failure load can be determined from Eqs. (2) and (3). If the nominal applied load is represented by P and the corresponding total strain energy release rate is G_T, the critical load for delamination initiation can be evaluated from

$$P_c = \sqrt{G_c/G_T}\,P \tag{9}$$

The critical load as a function of delamination length is plotted in Fig. 16 for the three ply-waviness angles studied. The critical load decreases as the delamination length increases for 0- and 4.8-deg waviness angles, whereas it remains flat for −4.8 deg. The scatter is smaller for the critical load as compared with the respective critical strain energy release rate because of the square root relationship

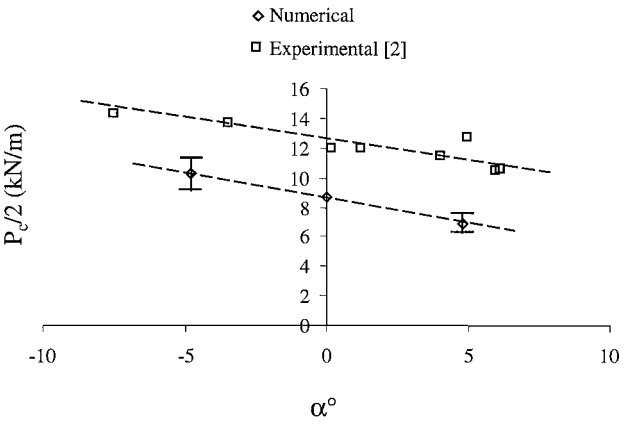

Fig. 17 Delamination initiation loads vs ply waviness angles (degrees).

between P_c and G_c [Eq. (9)]. The coefficient of variation for P_c is roughly one-half of the coefficient of variation for G_c. For delamination initiation prediction, the first set of values corresponding to the half-ply thickness delamination length should be used.

The experimental results in Ref. 3 and the present numerical predictions are plotted in Fig. 17. The present numerical analysis clearly captured the trend of the experimental results. The numerical results seem to show a slightly more pronounced ply waviness effect, which reflects that, at the critical location, the as-manufactured specimens have smaller taper angles than the idealized models. The predicted loads are consistantly smaller than the actual experimental loads, which can be attributed to that the idealized model has a larger resin pocket than the as-manufactured specimens. The larger the resin pocket, the lower the failure load should be.

Conclusion

Delamination initiation and growth was predicted for skin-stiffener structure under pull-off type loading using a fracture-mechanics approach. The example presented demonstrates the effective prediction of delamination failure using only fracture toughness test data. In addition, ply waviness was identified as a critical factor influencing the delamination failure load. As the ply waviness angle varies from −4.8 to 4.8 deg, the failure load decreases. The positive (including zero) waviness angle results in unstable delamination growth, whereas the negative waviness angle seems to produce stable delamination growth. The present numerical analysis captures the trend of available experimental results.

References

[1]Baker, D. J., Nunn, K. E., Rogers, C. W., Dompka, R. V., and Holzworth, R. C., "Design, Development and Test of a Low-Cost, Pultruded-Rod-Stiffened Wing Concept and Its Application to a Civil Tilt Rotor Transport," *10th DOD/NASA/FAA Conference on Fibrous Composites in Structural Design*, Vol. 2, 1993, pp. 125–167.

[2]Li, J., O'Brien, T. K., and Rousseau, C. Q., "Test and Analysis of Composite Hat Stringer Pull-Off Test Specimen," *Journal of the American Helicopter Society*, Vol. 42, No. 4, 1997, pp. 350–357.

[3]Li, J., and O'Brien, T. K., "Ply Waviness Effects on the Pull-Off Loads in Composite Hat Stringer Specimens," *Proceedings of the 14th U.S. Army Symposium on Solid Mechanics*, edited by K. Iyer and S.-C. Chou, Battelle, Columbus, 1996, pp. 173–185.

[4]Li, J., Lee, S. M., Lee, E. W., and O'Brien, T. K., "Evaluation of the Edge Crack Torsion (ECT) Test for Mode III Interlaminar Fracture Toughness of Laminated Composites," *Journal of Composites Technology and Research*, Vol. 19, No. 3, 1997, pp. 174–183.

[5]Reeder, J. R., and Crews, J. H., "Mixed-Mode Bending Method for Delamination Testing," *AIAA Journal*, Vol. 28, No. 7, 1990, pp. 1270–1276.

[6]Irwin, G. R., "Analysis of Stresses and Strains Near the End of a Crack Traversing a Plate," *Engineering Journal of Applied Mechanics*, Vol. 24, Sept. 1957, pp. 361–364.

[7]Rybicki, E. F., and Kanninen, M. F., "A Finite Element Calculation of Stress Intensity Factors by a Modified Crack-Closure Integral," *Engineering Fracture Mechanics*, Vol. 9, No. 4, 1977, pp. 931–938.

G. A. Kardomateas
Associate Editor